MobiChem: A Ubiquitous Smartphone-Based Toolkit for Practical Fruit Monitoring and Analysis

Zhiying Li[1,*], Abdul Aziz[2,*], Patrick Phuoc Do[2], Phuc Nguyen[2], Tianxing Li[1,†]
[1]Michigan State University, East Lansing, Michigan, USA
[2]University of Massachusetts Amherst, Amherst, Massachusetts, USA
{lizhiyi3,litianx2}@msu.edu,{abdulaziz,phuocdo}@umass.edu,vp.nguyen@cs.umass.edu

ABSTRACT

This paper introduces MobiChem, a low-cost, portable, practical, and ubiquitous smartphone-based toolkit for fruit monitoring. The key idea is to leverage the light emitted from a smartphone's screen and front camera, coupled with a custom-built screen cover, to perform comprehensive hyperspectral analysis on targeted objects. Specifically, we designed a zero-powered screen cover that selectively filters wavelengths essential for hyperspectral sensing. We then incorporate a CNN-based algorithm and a novel ranking-based learning technique that manipulates the latent space to classify maturity stages and characterize their chemical and physical factors. To demonstrate MobiChem's feasibility, robustness, and practicality, we showcase its application in tomato, banana, and avocado sensing. Our system examines the maturity, chlorophyll, lycopene content, free sugar levels, and firmness, enabling various dietary assessments and food safety applications. Experimental results using 117 tomatoes, 98 bananas, and 73 avocados show MobiChem achieved 95.67% accuracy in chlorophyll concentration measurement, 98.76% for lycopene detection, 93.53% for sugar concentrations analysis, and 91.34% average accuracy in classifying maturity (96.64% for tomato, 86.37% for banana, and 91.03% for avocado).

CCS CONCEPTS

• **Human-centered computing** → **Smartphones**; **Mobile phones**.

KEYWORDS

Fruit Sensing, Hyperspectral Imaging, Mobile Sensing

ACM Reference Format:
Zhiying Li, Abdul Aziz, Patrick Phuoc Do, Phuc Nguyen, Tianxing Li. 2025. MobiChem: A Ubiquitous Smartphone-Based Toolkit for Practical Fruit Monitoring and Analysis. In *The 23rd Annual International Conference on Mobile Systems, Applications and Services (MobiSys '25), June 23–27, 2025, Anaheim, CA, USA.* ACM, New York, NY, USA, 14 pages. https://doi.org/10.1145/3711875.3729135

∗ These authors contributed equally to this work.
† Corresponding author (litianx2@msu.edu).

MobiSys '25, June 23–27, 2025, Anaheim, CA, USA

ACM ISBN 979-8-4007-1453-5/25/06
https://doi.org/10.1145/3711875.3729135

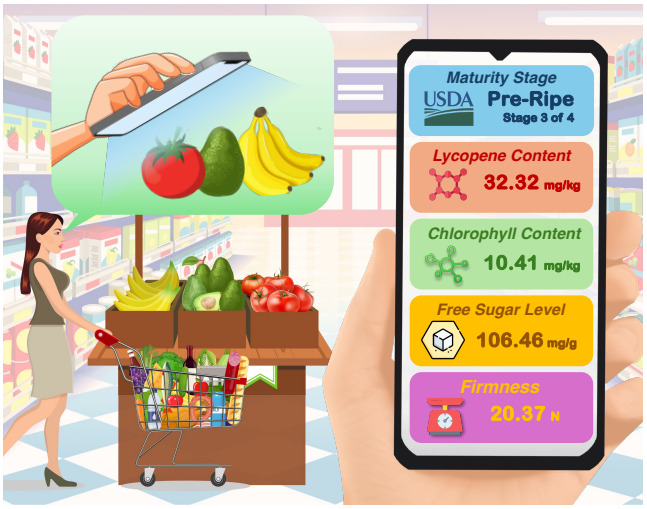

Figure 1: MobiChem Application Scenarios. The smartphone display illuminates, capturing a hyperspectral datacube through passive optical filters. It then analyzes maturity stage, chemical, or physical properties.

1 INTRODUCTION

In recent years, the expansion of global markets has significantly heightened the demand for high-quality fresh products. This trend emphasizes the critical need for rapid and accurate methods to assess fruit maturity. Assessing fruit maturity is a multifaceted process that involves analyzing factors such as color, internal quality, and firmness. For example, tomatoes and avocados are rich in many vitamins and minerals and contain bioactive compounds such as carotenoids, flavonoids, and phenolic acids, which contribute to their antioxidant properties [8, 23]. However, as the fruits ripen, they undergo significant physiological changes post-harvest [18]. This variability in maturity can lead to increased risks of spoilage in overripe fruits, causing considerable losses during transport and storage [53]. In addition, unripe fruits can cause stomach discomfort or constipation, while overripe fruits can lead to excessive sugar intake or fermentation [30].

Today's fruit monitoring methods, such as compression and puncture tests [41, 56], are destructive and can reduce the profitability of the produce by damaging the goods during the assessment process. Existing non-destructive techniques fundamentally adopt one of the two strategies: (a) radio-frequency (RF) sensing or (b) hyperspectral imaging (HSI). The former seeks to identify maturity indicators using magnetic resonance imaging (MRI) [29, 44], Wi-Fi [34], or Sub-Terahertz sensing [2]. The latter captures information in multiple wavelengths across the optical spectrum [28, 70, 72, 75, 79].

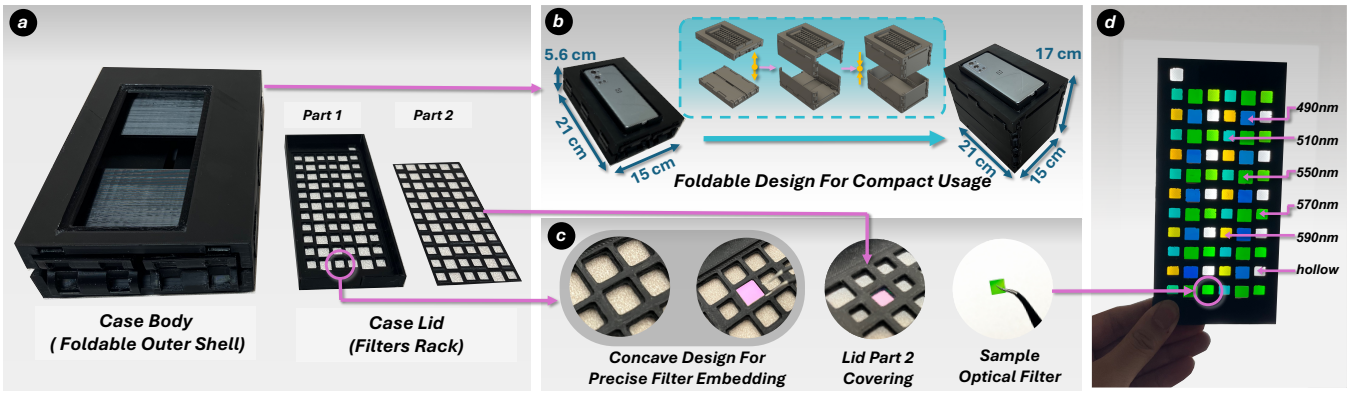

Figure 2: MobiChem Prototype: (a) A phone case with a lid to secure the filters, (b) A foldable design for enhanced portability and robustness, (c) A concave design for embedding filters, and (d) A case lid positioned beneath the lights.

However, these techniques remain not deployable for end-user applications in the foreseeable future due to their complexity and high cost, especially for everyday environments such as homes and grocery stores. Recent work proposed a smartphone-based hyperspectral imaging system (MobiSpectal [54]) for fruit sensing. However, MobiSpectal requires infrared cameras, which are not commonly found in today's smartphones. Their method involves substantial data collection and device calibration, rendering it impractical for commercial off-the-shelf (COTS) mobile devices. Additionally, the system can only perform coarse-grained fruit sensing (e.g., binary organic food classification), which limits its application scenarios. Therefore, a ubiquitous, low-cost, fine-grained, non-destructive fruit-monitoring mechanism has remained an open problem.

In this paper, we introduce MobiChem, a novel fruit monitoring system deployed on COTS smartphones with accuracy comparable to the gold-standard colorimeter-based approaches. As shown in Figure 1, MobiChem captures images across numerous narrow, contiguous optical bands, allowing for a detailed analysis of fruits by identifying subtle physiological changes that are not visible to the naked eye. Specifically, MobiChem reuses the phone screen to emit multiple narrow-band light spectrums toward the fruit. It utilizes the front-facing camera to capture the spectral profile of materials from reflected light, subsequently estimating fruit ripeness, chemical concentrations, and physical factors.

While the system's concept is clear, it needs to address two main challenges in COTS smartphone scenarios. First, the spectral resolution required for an accurate maturity assessment is typically achieved with expensive and bulky equipment like dedicated LEDs and prism. Second, it is nontrivial to estimate fruit ripeness and various chemical concentrations from a limited number of spectrum channels. Compared with commercial hyperspectral cameras that can produce over 200 narrow bands, MobiChem can only produce eight bands. To address these challenges, we first introduce a ubiquitous, foldable toolkit for mobile HSI using a low-cost, zero-power phone screen cover featuring custom 3D-printed cases and an automated filter selection process to expand illumination from three RGB wavelengths to broader spectral ranges. The toolkit enables reliable multispectral sensing compatible with COTS smartphones while optimizing portability, cost-efficiency, and ambient light blocking. We then develop two deep-learning models that accurately predict the chemical composition (chlorophyll, lycopene, sugar content) and physical properties (firmness) of fruits during ripening. Our deep learning framework comprises a robust maturity classification and a Rank-N-Contrast-based regression model to accurately predict chemical and physical properties, ensuring the system can handle imbalanced datasets and capture the non-linear relationships inherent in fruit ripening.

To examine the feasibility of MobiChem, we built a foldable (67% volume saving), compact (15 cm × 21 cm × 5.6 cm), and low-cost (<$50) prototype using off-the-shelf hardware components (Figure 2). Our prototype comprises an optical filter grid with eight narrow-band illumination from 463nm to 621 nm. We evaluated the prototype by sensing 117 tomatoes, 98 bananas, and 73 avocados.

The contribution of this paper is summarized as follows:

- To the best of our knowledge, MobiChem is the first to leverage the smartphone's front-facing camera and screen to perform hyperspectral imaging and sensing.
- We present a smartphone-based toolkit for mobile HSI utilizing a low-cost, zero-power phone screen cover. It incorporates an automated pipeline for custom hardware generation and a filter selection process that enables the expansion of illumination beyond the three RGB channels.
- We developed Rank-N-Contrast-based deep learning models leveraging hyperspectral images to capture subtle color and chemical composition differences in maturing fruits, enabling robust latent space alignment to capture the continuous and non-linear progression of biochemical transformations, outperforming traditional regression methods in modeling the ripening process.
- Experiments show MobiChem achieved 95.67% in chlorophyll measurement, 98.76% for lycopene detection, 93.53% for sugar concentrations, and 91.34% average in classifying maturity (96.64% for tomato, 86.37% for banana, and 91.03% for avocado).

Potential Applications. MobiChem's capabilities open the door to numerous innovative applications that have yet to be explored. Patients with diabetes can monitor their glucose levels by taking photos of their food with their smartphone, allowing better management of sugar intake. Farmers can monitor the growth stages and health of fruits, optimizing irrigation, fertilization, and pesticide use, and shoppers can assess the ripeness and quality of fruits before buying or consuming them.

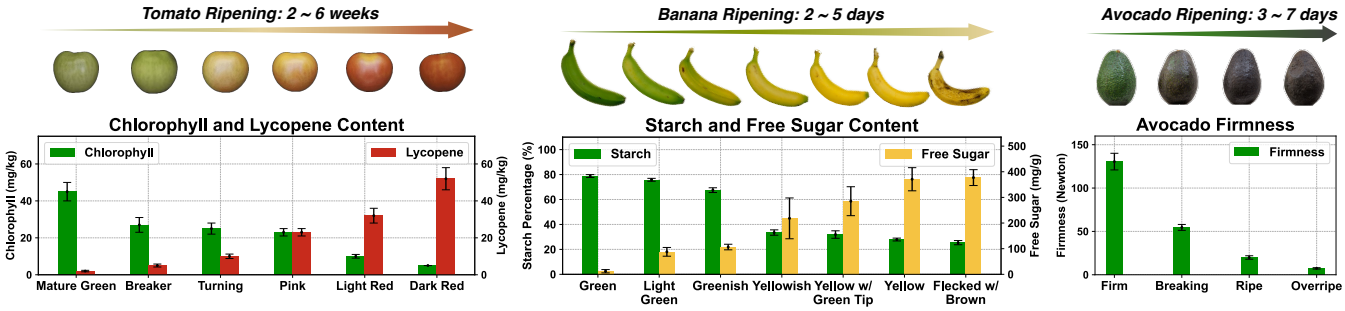

Figure 3: Post-Harvest Fruit Ripeness Based on USDA Guidelines: (Left) Six stages of tomato ripeness range from fully green to overripe [10, 33, 52, 76]. (Middle) Seven stages of banana ripeness range from green and firm to yellow and speckled [12, 22, 57]. (Right) Four stages of avocado ripeness range from hard and unripe to soft and ready to eat [42, 73]. (Fruits color figures online)

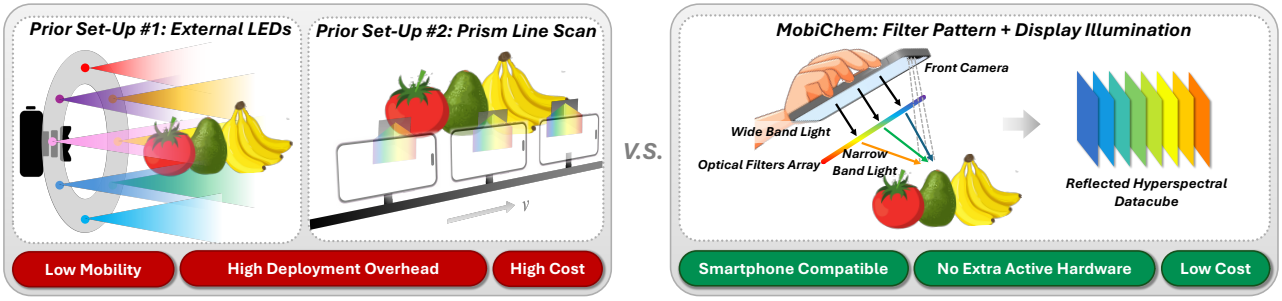

Figure 4: Comparison Between Existing Mobile Hyperspectral Imaging Systems (left) and MobiChem (right): Existing methods require costly and bulky optical components (e.g., external LEDs [20, 49, 71], prisms, and mechanical parts [43, 58, 59]). MobiChem reuses the smartphone's front camera and screen with narrow-band optical filters for accessible spectral sensing.

2 BACKGROUND AND MOTIVATION

Fruit Ripening. Fruits that continue to ripen naturally when stored at room temperature are known as climacteric fruits. Bananas, apples, mangoes, tomatoes, peaches, and avocados are all common examples of climacteric fruits. Climacteric fruits spans tropical and temperate regions, and are pervasive in groceries [3, 55]. Sensing fruit properties plays a crucial role in global agriculture and human diets because they continue to undergo biochemical changes and influence their texture, flavor, and nutritional profile. Figure 3 shows examples of tomatoes, avocados, and bananas turn from lighter to darker colors during ripening. The color transformation results from a combination of chemical changes (chlorophyll, lycopene, and sugar content) and physical factors (firmness) [47]. For example, tomatoes and tomato-based products are widely recognized as rich sources of chlorophyll and lycopene, offering significant health benefits [50]. Chlorophyll, a green pigment, is prevalent in plants and vegetables, while lycopene, a red pigment, belongs to the carotenoid family of phytochemicals. Regarding their reflection properties, lycopene exhibits primary absorption peaks at approximately 455-470 nm and 640-660 nm, whereas chlorophyll-a shows absorption peaks around 430-440 nm and 662-680 nm [7, 74].

Hyperspectral Imaging System. The hyperspectral imaging (HSI) system captures light across a broad range of wavelength bands, providing detailed spectral information about the target object. The finer-grained wavelength spectral profile enables HSI systems to be applied across various bio and agricultural fields, expanding their use beyond traditional computer vision techniques that use RGB images.

However, existing HSI systems rely on intricate optical components to disperse light across various regions of the scene (line or area scan), utilizing prism arrays and mechanical elements such as translational belts for accurate positioning. As shown on the left of Figure 4, existing methods rely on two system setups to obtain narrow-band spectral reflection: (a) using external LEDs [20, 49, 71] or (b) using prism line scan [43, 58, 59]. The *external LEDs* setup employs a standard camera sensor in a controlled lighting environment, using a combination of narrow-band light sources or a wide-band source modulated by a rotating filter wheel [48]. The setup selection is based on the availability and form factors of the camera sensor and illumination sources. Alternatively, a hyperspectral imaging system can also be achieved through the setup of *prism line scan*. This setup employs advanced camera configurations to filter selected spectral bandwidths reflected from a single wide-band light source. This mobile configuration can be achieved with miniaturized optical prisms or a customized CMOS sensor with more sensing bands than traditional RGB setups. Both setups require dedicated and expensive hardware, which are not commonly found in consumer devices, limiting their deployment on mainstream mobile devices.

Enabling HSI on standard RGB camera devices has the potential to broaden the scope of mobile sensing applications, significantly increasing their accessibility and adoption. To fill the research gap, we take advantage of the standard arrangement of the smartphone:

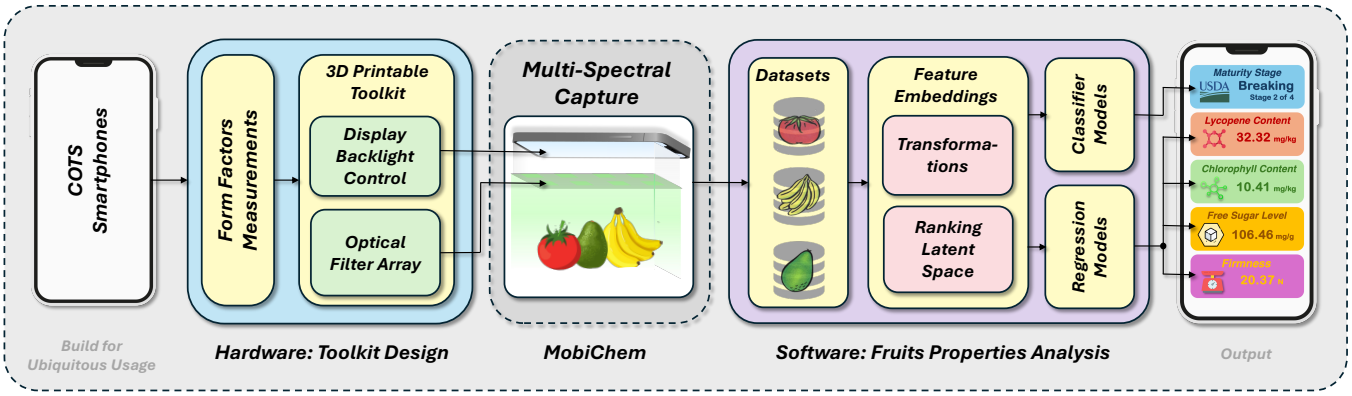

Figure 5: System Overview. It combines a customized smartphone-based toolkit with backlight controls and deep-learning models that optimize spectral data collection using feature embedding techniques to improve fruit property predictions.

the co-location of the front-facing camera and display. As illustrated on the right of Figure 4, we reuse the phone screen as the sole illumination source and the front-facing camera as the visual sensor. We then utilize narrow-band optical filters and tile them on the phone screen to achieve narrow-band lighting illumination. By modulating the camera capture time and position of light on and off according to the filter location, we can control each frame representing the narrow-band reflection at a particular wavelength.

3 MOBICHEM OVERVIEW

We propose MobiChem, which is compatible with widely available COTS smartphones and supports hyperspectral sensing. As shown in Figure 5, MobiChem consists of a *Smartphone-based Toolkit* hardware design and *Fruit Properties Analysis* algorithm.

Toolkit Design. The hardware module integrates a passive, foldable, and portable toolkit that can be easily attached to COTS smartphones for everyday use. The toolkit design module includes a phone-specific 3D printable outer shell and a custom backlight control application. First, geometric measurements, including phone dimensions, display size, camera position, and field of view, define the toolkit's outer shell and filter rack. Since MobiChem operates by utilizing the filtered backlight from the smartphone display, precise control over filter placement and modulation of display illumination is crucial during image capture. Second, the optical characteristics of the smartphone's display are examined, focusing on its spectral response at full brightness across each color channel. By accurately quantifying this response, narrowband filters can be simulated to generate additional spectral channels. These optical measurements optimize filter placement for uniform illumination at each narrowband wavelength. During continuous image acquisition, the backlight control application sequentially activates and deactivates specific filter regions for desired wavelengths.

Multi-Spectral Capture. After 3D-printing the hardware module, the user can simply place the optical filter array on top of the smartphone display, similar to a screen protector. The precisely engineered filter rack ensures accurate alignment of the filters corresponding to all wavelengths. Multispectral imaging is then achieved using the phone's front-facing (selfie) camera, with the synchronized activation and deactivation of specific filter regions on the display serving as the light source. During each HSI capture, MobiChem acquires a sequence of images of the same object under varying spectral illuminations. Since the system controls the wavelength of the light source for each frame, the data processing organizes the captured images into an HSI datacube format, with dimensions of height × width × spectral channels, for fruit maturity classification and regression tasks.

Fruits Properties Analysis. Since spectral sensing, in general, is advantageous in fruit analysis, MobiChem uses the raw multispectral images for the application of fruit property analysis. To boost the accuracy of fruit stage recognition, a feature embedding module is proposed to enhance the model performance and reduce the bias. This module uses the Rank-N-Contrast to map the raw input into a continuous feature space. In the end, the system is useful for inferring the properties of unseen fruit samples in terms of maturity stage, chemical concentration, and physical factors.

4 UBIQUITOUS TOOLKIT DESIGN FOR MOBILE HSI SYSTEM

We discuss MobiChem's smartphone-based toolkit for mobile HSI using a low-cost, zero-power, foldable phone screen cover here.

Implementing multispectral sensing on the mobile phone is challenging as there are not sufficient resources to realize robust light source transceivers like in traditional HSI systems. Smartphone displays are typically limited to three wide-band peaks in the red, green, and blue regions, but true multispectral systems require more distinct wavelengths. Furthermore, display dimensions, brightness, and RGB spectral signatures vary across different brands and models, complicating the development of a universal method to derive sufficient narrow-band illuminations from three-peak RGB sources.

To tackle these challenges, we introduce a pipeline process to generate custom hardware compatible with COTS smartphones and enable them to perform hyperspectral analysis reliably. Figure 6 illustrates the hardware generation pipeline, consisting of two primary components: (1) custom 3D-printed cases for sample placement, designed to align with the light path and display characteristics of the smartphone camera, and (2) a filter selection process that utilizes optical filters customized for the phone screen.

The pipeline for 3D-printed cases begins with gathering details about the smartphone's form factor, such as height, width, camera

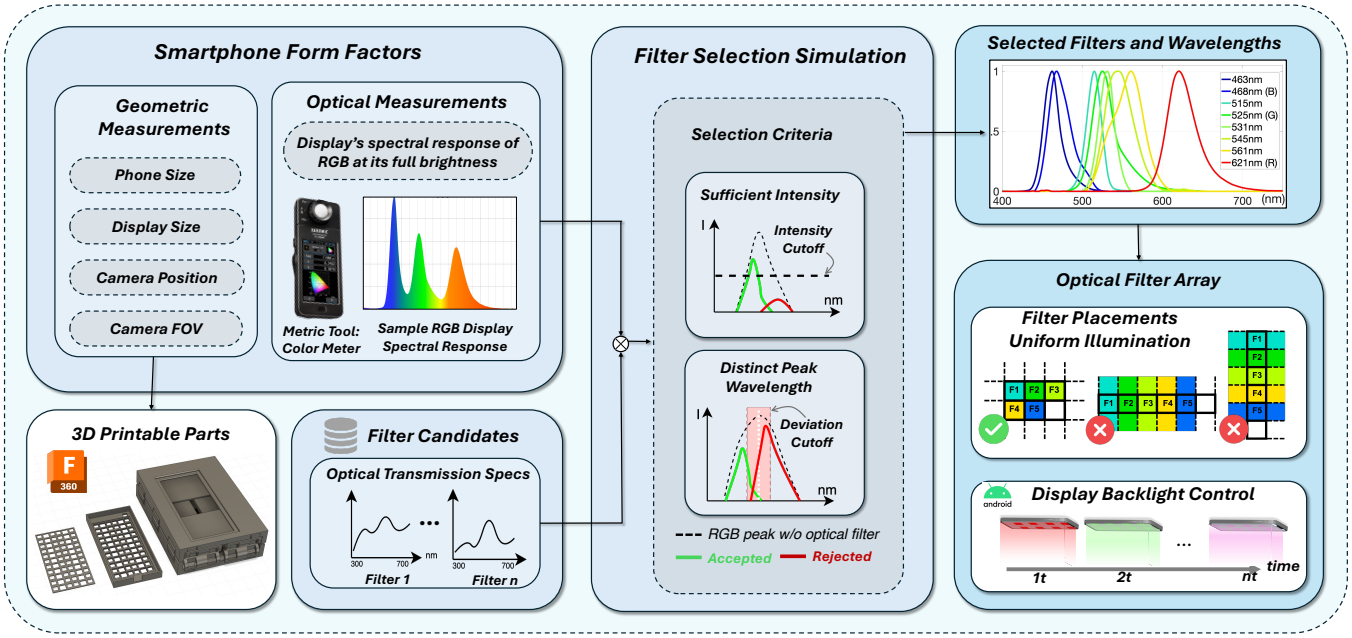

Figure 6: Flowchart for Generating Passive Toolkit Add-on of MobiChem. The pipeline consists of two main components: (a) custom 3D-printed cases designed to align with smartphone camera specifications and (b) a filter selection process that uses optical filters to expand illumination wavelengths beyond standard RGB.

position, and field of view. These parameters can be obtained from the phone's technical specifications or easily measured. Using an automated geometric generation routine, the system quickly calculates the dimensions for a customized 3D model tailored to the specific smartphone and sensing application. Printing these phone cases with entry-level 3D printers costs under $10 in filament. We optimized the box volume with a foldable design (Figure 2b), reducing its size from 15×21×17 cm to 15 × 21 × 5.6 cm—a 67% reduction.

The filter selection process addresses the challenge of expanding illumination from three RGB wavelengths to a broader range. This involves automatically identifying suitable optical filters tailored to the smartphone. The process begins with obtaining the phone display's optical metrics and the front-facing camera's sensitivity range, information readily available from technical specifications or measurements. As shown in the middle of Figure 6, it involves choosing from a pool of filter candidates. There are two types of filters: plastic and glass. Plastic filters, made by injecting dyes, are easy to cut and offer a wide range of options, allowing for more combinations to shift the RGB peak of different display lights and generate new wavelength peaks [14]. However, their transmission rates can be irregular. In contrast, glass filters operate based on the Fabry-Perot cavity principle, providing precise narrow-band transmission rates but being more rigid in shape [19].

The selection of optimal filters follows two criteria: (1) a minimum intensity cutoff to ensure sufficient illumination power and (2) a minimum center peak wavelength deviation from RGB to guarantee that the selected spectral differ from the original RGB lights. These criteria ensure effective brightness and spectral coverage.

Using the OnePlus 8 Plus as an example, we identified five narrow-band filters with optimal wavelengths, enabling the creation of eight distinct illumination sources when combined with the phone's original RGB peaks. The filter selection process is customized based on the RGB peaks and specific filter properties. To begin, we measured the phone's bright light spectrum without any filter using a Sekonic C-7000 Spectrometer [46]. Next, we obtained the band-pass ratios of the filters at different wavelengths from their vendor's specifications. We considered two filter options: ROSCO plastic filters [16] and narrow-band optical glass filters [67], both priced at approximately $0.02 per square inch. A total of over 180 filters were selected as candidates. Using the RGB spectral profile and the filters' band-pass characteristics, we simulated the resulting peak wavelengths and intensities through an automated filter selection process. The a minimum intensity cutoff was set as 20% and minimum center peak wavelength deviation, 5nm. Ultimately, we identified eight distinct wavelengths—463nm, 468nm(blue), 515nm, 525nm(green), 531nm, 545nm, 561nm(red), and 621nm—as shown in Figure 6 and Table 1.

Filter	Peak wl	FWHM	Screen Backlight	Resulting wl
[62]	490 nm	30 nm	blue (468 nm)	**463 nm**
[63]	510 nm	20 nm	green (525 nm)	**515 nm**
[64]	550 nm	20 nm	green (525 nm)	**531 nm**
[65]	570 nm	25 nm	green (525 nm)	**545 nm**
[66]	590 nm	40 nm	green (525 nm)	**561 nm**

Table 1: Selected Filters for the display of OnePlus 8 Plus

Beyond the filter selection process, we optimize smartphone camera settings by adjusting the front camera's capture time and controlling the backlight area at specific filter positions aligned with the hardware-mounted filter locations. To ensure consistency, we fix camera parameters such as exposure time, ISO, and frame duration, maintaining uniform settings across all captured images.

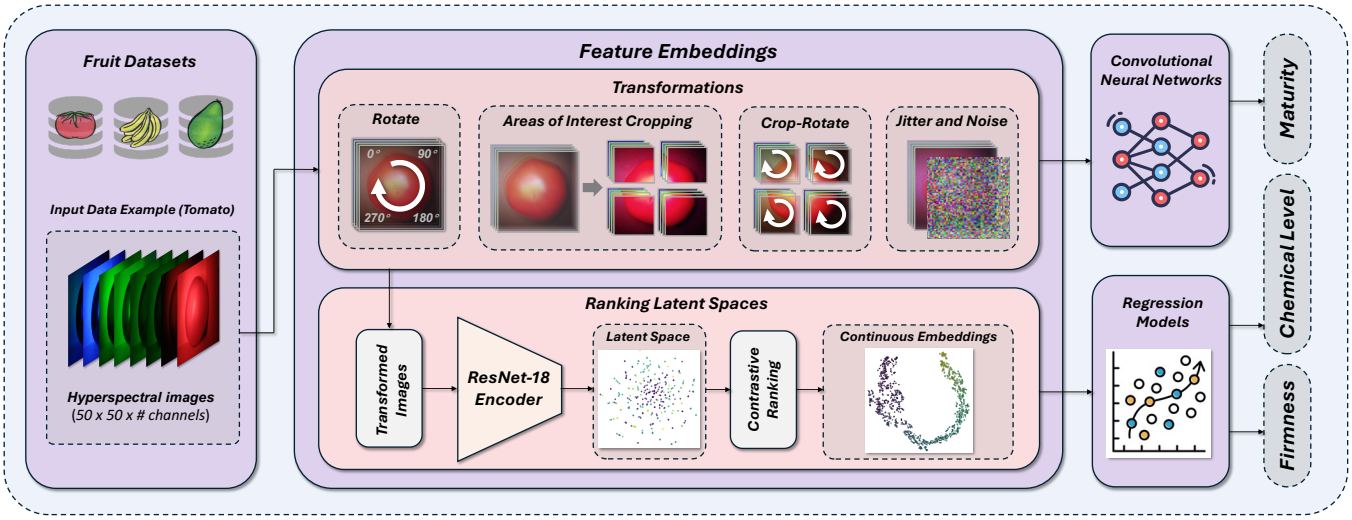

Figure 7: Classification and Prediction Schemes. The images are first augmented via transformations and passed to the convolutional neural network and regression models. (1) The convolutional neural network extracts features from input images and classifies maturity stages. (2) In the latent space, the transformed images first train an encoder with the contrastive ranking-based loss function that reflects the continuous nature of the target variable. (3) The linear regressor is then trained on top of the encoder using L1 loss to predict the chemical concentrations or physical properties.

Auto-exposure, auto-focus, and auto-white balance are disabled to prevent automatic adjustments during image capture. If the camera's internal hardware allows for precise control, all photographic parameters are standardized. Additionally, we designed a foldable phone case to embed the filter (Figure 2), enhancing portability and effectively blocking ambient light. When the screen is off, the illumination within the phone case remains below 5 lux, ensuring low light levels during data collection.

5 MATURITY DETECTION AND FRUIT PROPERTIES ANALYSIS

This section provides a detailed discussion of the classification and regression of fruit maturity, chemical and physical properties.

5.1 Classifying Fruit Maturity Stage

Maturity classification involves assigning fruits to discrete categories. For example, for tomato, there are "mature green", "breaker", or "dark red", etc. These categories represent distinct stages in the ripening process, which are characterized by unique spectral response in the hyperspectral images captured by MobiChem. We propose a Convolutional Neural Network (CNN) model for our classification task. CNNs are particularly well-suited for this task because they excel at learning hierarchical features directly from complex raw image sources, enabling effective discrimination between these discrete classes.

To ensure consistency across different fruit types, we adopt a single CNN architecture for all fruits in our experimental setup. The model consists of three 2D convolutional layers with 32, 64, and 128 filters, each followed by batch normalization, ReLU activation, and max pooling to extract complex image features. The features are flattened and passed through two fully connected layers with 128 and 256 units, followed by a dropout layer (probability 0.5) to prevent overfitting. The nodes on the output layer correspond to the different maturity stages of the fruit being tested. We trained the model using the Adam optimizer and a weighted loss function $LF = -\alpha_t(1-p_t)^{\gamma}log(p_t)$ where p_t is the model's predicted probability for the true class, α_t is the weighting factor for each class and is set to be inversely proportional to the class frequencies, and γ controls the weighting of hard-to-classify samples. This loss function approach addresses the issue of data imbalance by putting more focus on hard-to-classify samples, thereby enhancing model performance and reducing class bias.

However, each fruit type exhibits its own set of maturity stages with distinct spectral profiles. For instance, tomatoes are classified into six stages, while avocados are classified into four, as shown in Figure 3. To account for these differences, we train separate instances of the CNN for each fruit type. This approach allows the model to be finely tuned to the specific spectral characteristics and ripening patterns of each fruit, ensuring high classification accuracy tailored to the fruit's unique maturity progression. But we ensured consistency in training procedures across all the fruit-specific CNN instances by following identical data splitting (80-20 train-test split), the same augmentation methods, and standard hyperparameter tuning approaches.

5.2 Prediction of Chemical Concentrations and Physical Properties

Another key component of MobiChem is its ability to accurately predict the chemical composition and physical properties of fruits during different maturity stages. The comprehensive spectral data captured by our proposed system provides insights into the internal composition of fruits, which are not discernible in conventional RGB images [81]. Our goal is to establish a correlation between the acquired spectral data with the chemical (chlorophyll, lycopene, and sugar content) concentrations and the physical properties of fruits (firmness). Our experiments with tomatoes, bananas, and

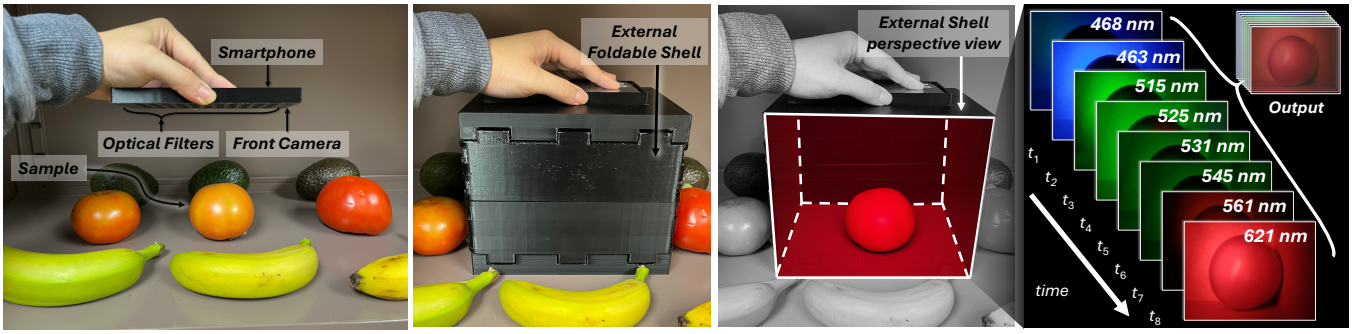

Figure 8: MobiChem Multi-Spectral Capture Experimental Settings

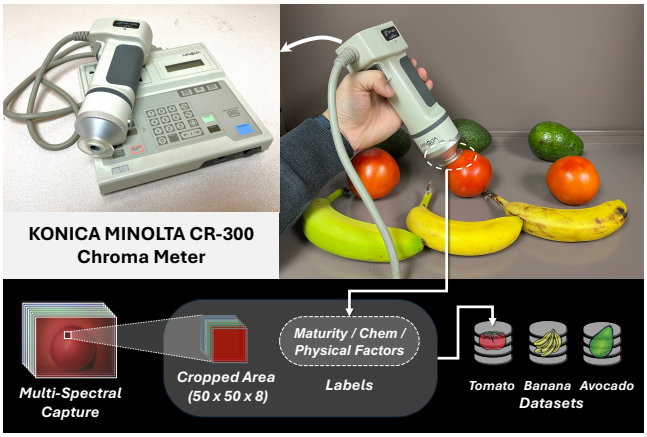

Figure 9: Ground Truth Collection Settings

avocados showed that they undergo complex and non-linear biochemical transformations during ripening. In tomatoes, lycopene synthesis intensifies during mid-ripening, changing the fruit's color from green to red [31]. Bananas convert starch to sugars, leading to a rise in sugar content [37], and avocados feature an increase in oil content [6]. This causes non-uniform, and continuous changes in the fruits' chemical composition and physical properties as they mature (Figure 3). For the prediction of these chemical concentrations, we utilize a regression model based on the Rank-N-Contrast (RNC) framework [80].

Unlike maturity classification, which deals with discrete stages, concentration prediction requires estimating the continuous values of the chemical changes that occur during the ripening process. Traditional regression methods struggle to model these processes effectively. Linear regression and machine learning techniques (such as Support Vector Regression) attempt to fit a general relationship between the input hyperspectral data and the target chemical concentrations. However, these methods fail to capture the sigmoidal or exponential patterns characteristic of ripening, struggling to use the temporal or stage-wise progression relationships of the natural continuity during the ripening process. As a result, they produce fragmented and inconsistent predictions.

We integrated the RNC framework into our predictive system to capture the continuous and ordered character of fruit ripening. Unlike traditional regression methods, the RNC framework is ideally suited for this task because it maps hyperspectral data into a latent space where embeddings reflect the ordered progression of ripening. This method explicitly optimizes the feature embeddings to match the desired chemical and physical properties. RNC enforces similarity alignment in the embedding space that represents the maturity progression by ranking samples based on their target distances and contrasting each sample against others. For instance, samples representing early-stage green tomatoes are positioned closer in the embedding space, while mid-ripening samples are progressively distanced to align with their distinct biochemical transformations. By suppressing spurious features and capturing the natural trend of ripening, this ordered embedding helps the model focus on meaningful variations. Specifically, we implement a two-stage approach that combines deep learning with the refined capabilities of the RNC method, as illustrated in Figure 7.

For each fruit type, we train a single RNC model. First, we train a deep neural network encoder based on a modified ResNet-18 architecture to extract high-dimensional features from our hyperspectral images [26]. The encoder is adapted to process our input size of 50×50 pixels across eight spectral channels, as opposed to the standard ResNet-18, designed for 224×224 pixel RGB images. We modified the architecture to increase the input channel depth from three to eight in the initial convolutional layers, adjusting filter sizes in deeper layers, and adapting the network to accommodate smaller spatial dimensions. This customized architecture enables the model to capture crucial spectral and spatial features related to chemical content and physical properties in the fruit. The model is then trained using a ranking and contrastive loss function, which organizes the images based on their chemical content and physical properties. Initially, the labels group images with similar chemical and physical characteristics, providing a reference framework. The contrastive learning mechanism then leverages this framework to adjust the embeddings, ensuring that samples with similar labels are closer to the latent space. In contrast, samples with significantly different concentrations are pushed further apart. This approach captures the intrinsic order within the data, reflecting the gradual changes in chemical content and physical properties during the ripening process. Once the encoder is trained, we freeze its weights and use the extracted features as input to a linear regressor. This regressor maps the latent space representations to the actual values of chemical content and physical properties using L1 loss. To enhance robustness, we incorporate data augmentation techniques and regularization during training.

However, we found during our experiments that applying a single set of hyperparameters universally across all regression tasks

Fruit / Prediction Task	Tomato			Banana			Avocado		
Input	MobiChem	RGB	+/-	MobiChem	RGB	+/-	MobiChem	RGB	+/-
Classification Accuracy	96.94%	78.33%	**18.61%**	86.37%	72.32%	**14.05%**	91.03%	78.97%	**12.06%**

Table 2: Maturity classification accuracy for tomato, banana, and avocado using MobiChem or RGB Inputs

Fruit	Tomato						Banana			Avocado		
Prediction Task	Lycopene			Chlorophyll			Sugar Content			Firmness		
Input	MobiChem	RGB	+/-	MobiChem	RGB	+/-	MobiChem	RGB	+/-	MobiChem	RGB	+/-
Regression R^2	98.76%	92.31%	**6.45%**	95.67%	87.34%	**8.33%**	93.53%	72.32%	**21.21%**	81.27%	78.04%	**3.23%**

Table 3: Regression R^2 for detecting chemical concentration and firmness using MobiChem and RGB inputs.

(chlorophyll, lycopene, sugar content, and firmness) resulted in suboptimal performance due to differences in the spectral and chemical signatures specific to each attribute and fruit type. Thus, we performed targeted hyperparameter tuning for each regression model to accommodate distinct chemical and physical characteristic profiles. Specifically, we set the learning rate of the encoder to 0.01 for tomatoes and bananas and 0.1 for avocados. The model predicting tomato lycopene concentrations was trained for 3,000 epochs while the other models used to predict chlorophyll, sugar content, and firmness ran for 5,000 epochs. The SGD optimizer was used with the specified initial learning rates, a learning rate decay of 0.1, weight decay of 1e-4, and momentum of 0.9. The RNC loss function was further configured using a temperature parameter of 2, with L1 as the label distance function and L2 as the feature similarity function. A uniform batch size of 64 was applied in all experiments to ensure consistency. For the linear models across all fruits, we employed a batch size of 128, trained for 2,000 epochs, and used an initial learning rate of 0.1 with the same decay, weight decay, and momentum settings. These hyperparameters were determined based on the coefficient of determination, R^2, observed during the training process for each fruit's dataset. This ensures that our regression model is optimized for each fruit type.

6 EVALUATION

In this section, we begin by evaluating MobiChem's performance in fruit maturity classification and regression against the gold-standard ground truth, showcasing its potential for innovative mobile applications. This is followed by a detailed presentation of monitoring chemical concentrations (lycopene, chlorophyll, and sugar content) and physical properties (firmness).

6.1 Experimental Settings

Data Collection Using Real Fruits. We monitor tomatoes, avocados, and bananas for our experimental analysis. MobiChem's functionality can be extended to other fruits or objects with similar properties. To conduct experiments on real fruits with ground truth measurements for maturity, chemical content (lycopene, chlorophyll, and sugar content), and physical factor (firmness), we initiated the study by acquiring fruits of each type in stage 1 (unripe) according to Figure 3. These fruits were carefully selected to ensure uniformity at the starting stage of ripeness. Our goal was to capture the full spectrum of ripening, from the initial stages to full maturity, thus providing comprehensive data for analysis.

Figure 8 summarizes the data collection process. For tomatoes, natural ripening was monitored closely, with 5–6 regions measured per fruit to account for internal variation. This process included 117 tomatoes across six maturity stages, with both RGB and hyperspectral images captured equally for each region. For bananas, ripening was documented from the green stage to fully ripe with brown flecks, focusing on starch-to-sugar conversion and chlorophyll degradation. Data from several peel regions produced a dataset of 98 bananas at seven ripening stages, with equal RGB and hyperspectral imaging emphasizing spectral and visual changes. Avocado ripening, characterized by firmness reduction and oil accumulation, was documented across four maturity stages. Unlike tomatoes and bananas, avocados show minimal color change, so the focus was on subtle firmness and spectral variations. The dataset included 73 avocados, with RGB and hyperspectral images captured from various parts of each fruit.

We randomly shuffled the list of fruits and split them into independent training and testing sets using standard machine learning practice. 80% was kept for training and 20% for the test set. To avoid data leakage, we separated the fruits so that a sample from a fruit in the training set did not appear in the test set. We also ensured that samples from the same fruit were kept within their original set for all of its maturity stages.

Ground Truth. We used a KONICA MINOLTA CR-300 Chroma Meter [39], which has been widely used in previous studies [1, 5, 68], as illustrated in Figure 9, to correlate colorimeter readings with maturity grading, lycopene, chlorophyll, sugar content, and firmness in real fruits. We connected the accurate, objective color data from the device to the internal biochemical changes in the fruits. This method enabled accurate tracking and analysis of ripeness progression in our samples.

For each sample, the Chroma Meter ground truth measurement (Figure 9) and MobiChem capture (Figure 8) occur sequentially, with a time gap under 2 minutes to ensure consistency. During ground truth measurement, 4—6 random scanning areas per fruit are recorded for reference. For MobiChem capture, each area is cropped into a 50×50×8 datacube and stored with its corresponding label. Each fruit is measured 2–5 times to track ripening with at least a 2-day gap. The final dataset includes 2,248 samples from 117 tomatoes, 1,568 from 98 bananas, and 1,168 from 73 avocados, covering multiple ripeness stages.

We used existing research [1, 5, 76] to convert Chroma Meter readings into maturity stages and lycopene/chlorophyll concentrations for tomatoes. For avocados and bananas, once maturity was determined, sugar content and firmness were interpolated from relationships in [12, 42, 57, 73, 75].

Evaluation Metrics. We use the following metrics in the evaluation, commonly used in fruit monitoring.

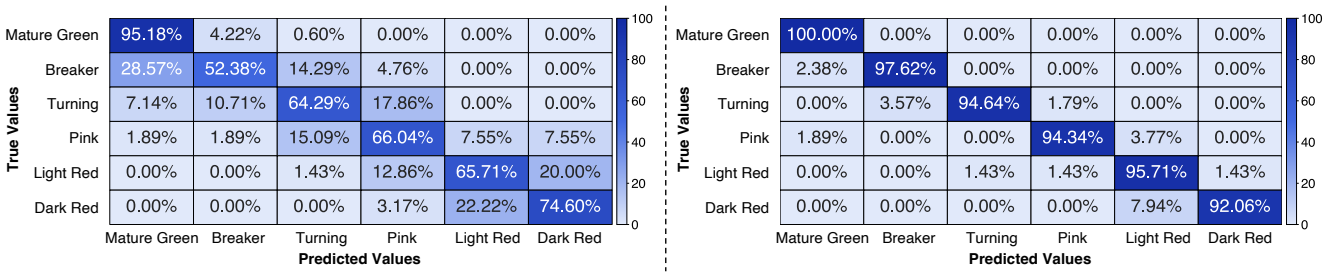

(a) ***RGB*** **Model** (b) ***MobiChem*** **Model**

Figure 10: Confusion Matrix for Tomato Maturity Classification. (a) The RGB Image Model shows significant misclassification at all maturity stages. (b) The 8-channel HSI Model shows noteworthy improvement over the RGB model for each ripeness level, indicating the effectiveness of additional spectral information.

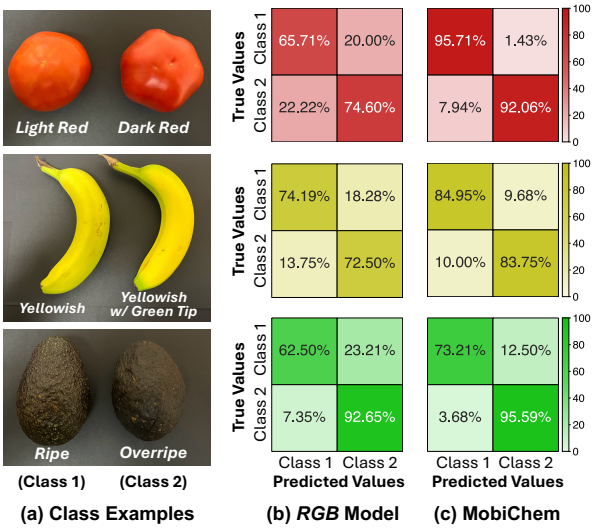

(a) Class Examples (b) ***RGB*** **Model** (c) MobiChem

Figure 11: Comparing RGB and MobiChem Inputs for Fruit ripeness Classification. (a) Sample images show subtle visual differences between classes. (b) RGB-based models exhibit high false positives and false negatives. (c) MobiChem demonstrates better class separation with much improved accuracy.

- For fruit maturity experiments, we measure the absolute maturity classification error between the estimated maturity stages and ground truth.
- For the experiments on chemical concentrations and physical properties, we leverage the coefficient of determination (R^2) as the primary criterion to enable comparison with existing studies [5, 15, 77]. The formula of R^2 is defined as Eq. 1:

$$R^2 = 1 - \frac{\sum_{k=1}^{m}(\hat{y_k} - y_k)^2}{\sum_{k=1}^{m}(\hat{y_k} - \bar{y})^2} \tag{1}$$

where $\hat{y_k}$ and y_k are the ground truth and estimated value of the k^{th} chemical concentration or physical properties, respectively. m is the total number of experiment samples. $\bar{y}$ is the mean value of the ground truth. The coefficient of determination $R^2 = 1$ if the predicted value y_k exactly matches the observed value $\hat{y_i}$. $R^2 < 0$ indicates that the system is worse than using the mean of the observed values.

Baselines. In the evaluation, we consider two baselines: first, traditional RGB photos to estimate fruit maturity, chemical concentrations, and physical properties (§6.2), and second, MobiSpectral [54], a recent mobile HSI system for fruit monitoring achieved by software-level spectral upsampling from RGB-I images (§6.3).

6.2 Overall Performance

Maturity Stages Classification. In this experiment, we compared the maturity stage classification accuracy using MobiChem (8-channel HSI) and traditional RGB images. The results in Table 2 clearly show the advantage of MobiChem for maturity classification across all three fruit types—tomatoes, bananas, and avocados, emphasizing the value of additional spectral information in capturing the biochemical and physical changes during fruit ripening. For tomatoes, MobiChem achieved 96.94% accuracy, surpassing the 78.33% accuracy using RGB inputs. For bananas, MobiChem's accuracy was 14.05% higher than RGB, showing it is better at handling complex ripening processes, such as starch-to-sugar conversion and uneven chlorophyll breakdown. RGB inputs struggle in stages with less distinct visual transitions (e.g., early green-to-yellow), while MobiChem provides more robust spectral signatures to differentiate these stages. For avocados, MobiChem achieved 91.03% accuracy, outperforming RGB inputs at 78.97%, representing a 12.06% improvement. During ripening, avocados exhibit subtle changes like oil accumulation and hardness loss, which are challenging to detect with RGB imaging but are captured effectively with hyperspectral imaging. This indicates that MobiChem's enhanced spectral resolution allows for detecting subtle variations in biological characteristics, helping to differentiate between ripening phases.

The detailed confusion matrices in Figure 10 further illustrate the differences in stage-wise classification performance between RGB and MobiChem models for tomatoes. As shown in Figure 10(b), MobiChem achieved an accuracy of 96.94% across all stages. In contrast, the RGB image classification method proved less effective overall, achieving an accuracy of only 78.33%. Figure 10(a) shows more significant misclassifications across all maturity stages, particularly at intermediate ripening stages. For the 'Breaker' stage, only 52.38% are correctly classified, with 28.57% misclassified as 'Mature Green' and 14.29% as 'Turning'. For the 'Turning' stage, only 64.29% are correctly classified, with 7.14% misclassified as 'Mature Green' and 10.71% as 'Breaker'. However, the MobiChem model exhibits notable advancements at every level. The misclassification

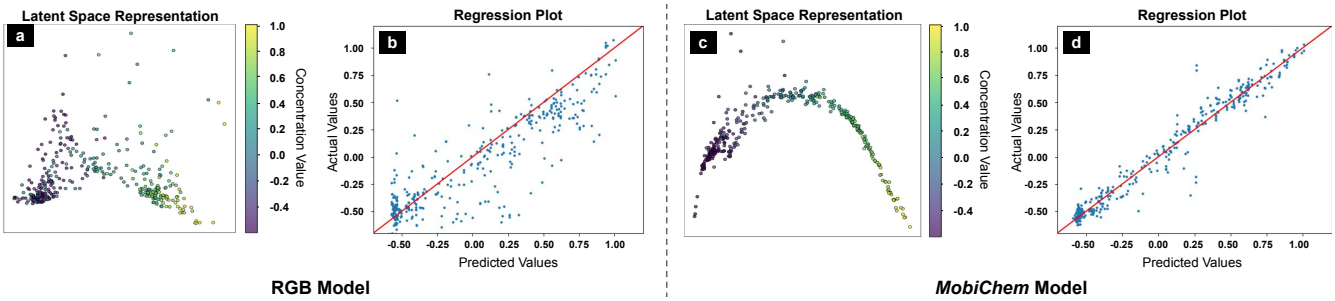

Figure 12: Result of predicting lycopene concentration using MobiChem. (a) The latent space of the RGB Model shows more scattering of the data. (b) A less organized latent space means the regression results are also more spread around the diagonal line. (c) The latent space for MobiChem has very little scattering of the data. (d) This results in a tighter regression plot and more accurate results.

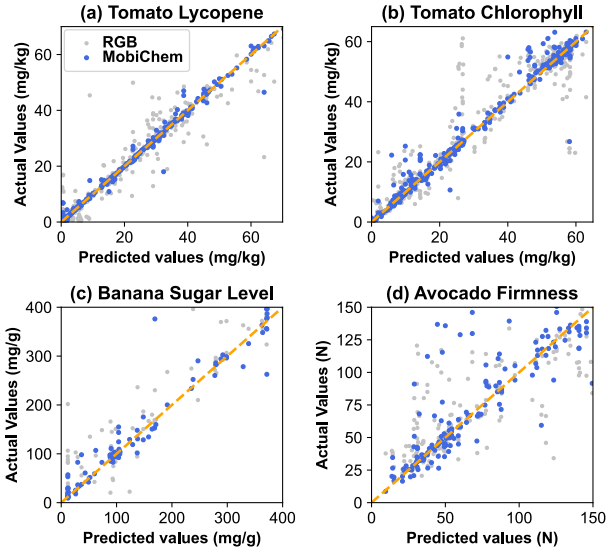

Figure 13: Regressor Prediction using MobiChem vs. RGB: (a) Tomato lycopene concentration (b) Tomato chlorophyll content (c) Banana sugar level (d) Avocado firmness

as 'Mature Green' for 'Breaker' drops to 2.38%, and the 'Breaker' stage improves significantly to 97.62%. With an accuracy of 45.26%, the 'Turning' stage demonstrates the model's capacity to resolve intermediate phases. Accuracy in the late phases, such as 'Pink' and 'Light Red', also improves, with 94.23% and 95.71%, respectively, compared to 66.04% and 65.71% for the RGB model. The final 'Dark Red' stage achieves 92.06% accuracy, reducing misclassification significantly. In addition, if we analyze some adjacent states, we can tell by side-by-side sample comparison for fruit samples, the precise stage is difficult of user to identify in real scenario, and mostly for many RGB image based CV system. Figure 11 is an ablation view of the tomato, banana and avacado confusion matrix at visually similar adjacent stages. These stages are essential to distinguish. For example, tomatoes contain the richest Lycopene content at the full red stage, and avocados have the most oil content at the Ripe stage instead of the overripe stage. However, through side-by-side comparison of the MobiChem vs RGB input for the classification task, MobiChem proves it has better precision to distinguish between these easily confused classes.

The comparison demonstrates the superiority of HSI over RGB for classifying tomato maturity stages. MobiChem leveraged additional spectral information captured by the 8-channel methods, providing crucial data, particularly in stages where color differences are subtle, to achieve higher classification accuracy. These findings validate our approach of using hyperspectral filters with smartphones to capture detailed spectral data, significantly enhancing the accuracy of tomato maturity stage determination compared to traditional RGB imaging techniques.

Chemical Concentration and Firmness Prediction. Table 3 summarizes the regression R^2 values for predicting chemical concentrations and physical properties across tomatoes, bananas, and avocados using MobiChem and RGB inputs. MobiChem consistently outperforms RGB models across all tasks and fruit types, highlighting its ability to capture subtle spectral features that RGB models fail to detect. Lycopene prediction in tomatoes achieved an R^2 of 98.76% with MobiChem, compared to 92.31% for RGB, reflecting a 6.45% improvement. Similarly, chlorophyll prediction yielded R^2 values of 95.67% for MobiChem versus 87.34% for RGB, with an 8.33% improvement. For the sugar content in bananas, MobiChem achieved an R^2 of 93.53%, compared to 72.32% for RGB, with a 21.21% improvement. For avocado firmness prediction, MobiChem achieved an R^2 of 81.27%, representing a improvement of 3.23% over RGB's value of 78.04%.

MobiChem's hyperspectral imaging captures fine-grained spectral information, leading to better latent space organization and clustering, as shown in Figure 12. In the RGB model (Figure 12(a)), we can see a relatively scattered distribution of points in the latent space representation and a less clear separation between different lycopene concentration levels. In contrast, the 8-channel HSI latent space (Figure 12(c)) has a more organized and distinct clustering with a smooth color gradient from purple to yellow, indicating a better alignment of lycopene concentration values. This organized clustering highlights *MobiChem's* ability to capture detailed spectral nuances. Because of this, the scatterplot of the actual versus predicted results for MobiChem (Figure 12(d)) exhibits a tighter clustering of values around the diagonal line, indicating higher prediction accuracy than the scatterplot for RGB (Figure 12(b)).

The improved R^2 values across all fruits and properties, which reflect MobiChem's consistent ability to extract meaningful spectral data correlating with target attributes. The scatterplots for MobiChem (Figure 13) further illustrate its tighter alignment with

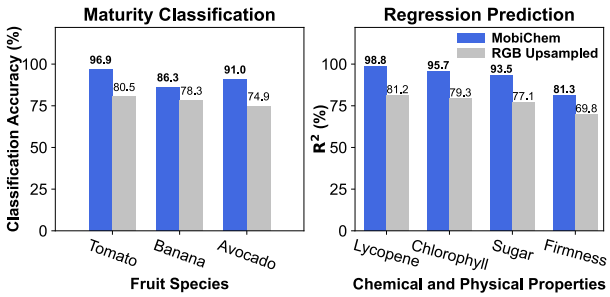

Figure 14: Comparison with Spectral Reconstruction: We replicated the RGB up-sampling algorithm from MobiSpectral and performed experiments to benchmark the performance in (left) classification and (right) regression tasks.

actual values, in contrast to the broader dispersion seen with RGB. This demonstrates MobiChem's precision and reliability in both chemical and physical property predictions.

6.3 Comparison with Spectral Reconstruction

In this section, we compare MobiChem with MobiSpectral [54], a phone-based hyperspectral imaging system using MST++ [9] for spectral reconstruction. Unlike MobiChem, which uses filters to retrieve spectra, MobiSpectral relies on a generative model to up-sample from RGB data. We evaluate classification and regression accuracy between MobiChem's eight spectral channels and MobiSpectral's transformer-upsampled channels.

Experimental Settings. We compare the classification model (§5.1) and regression model (§5.2) using two inputs: (1) MobiChem's 8-channel data samples (50×50×8) and (2) 40-channel datacubes up-sampled from RGB data (50×50×40). Both use the same test-train split, epochs, and learning rate, with MobiChem following the settings in (§6.1). We trained the MST++ transformer for spectral reconstruction using the open-source MobiSpectral dataset, which includes five fruits: tomato, kiwi, apple, blueberry, and strawberry. Since the application domain is in visible range, we modified the original model to take three-channel RGB and outputs 40 channels, covering the 400–700nm visible spectrum.

Result. As shown in Figure 14, MobiChem outperforms the existing solution, improving classification accuracy by 13.5% and R^2 by 20.6%. This indicates that MobiChem's 8-channel output provides richer data than MobiSpectral's RGB-based spectral reconstruction. Additionally, comparing with Table 2, MobiSpectral results closely match those from RGB, suggesting spectral reconstruction adds insufficient additional information for our learning models.

6.4 Ablation Study

To assess MobiChem's robustness and key components, we conducted an ablation study on fruit maturity classification and chemical/physical property prediction. Each ablated model was trained and tested using the same dataset and protocols as the full models (Sections 5.1 and 5.2) for consistency.

Maturity Classification Model. For the classification model, we tested the following modifications to the CNN: (1) variation in network depth (2, 3, or 4 layers), (2) adjustment of network width (16-32-64/32-64-128/64-128-256), (3) substitution of ReLU with LeakyReLU, and (4) removal of dropout regularization. Table 4 shows the results.

Ablation	Tomato	Banana	Avocado
***MobiChem* Model**	**96.94%**	**86.37%**	**91.03%**
2 Layer CNN	94.44%	82.17%	88.98%
4 Layer CNN	96.89%	82.80%	88.46%
16-32-64 Network	90.00%	81.85%	89.32%
64-128-256 Network	97.03%	87.58%	89.32%
Leaky ReLU	96.22%	86.31%	90.17%
No Dropout	94.44%	83.76%	88.46%

Table 4: Ablation study: Accuracies for maturity classification in tomatoes, bananas, and avocados

Ablation	Lycopene	Chlorophyll	Sugar	Firmness
MobiChem	**98.76%**	**95.67%**	**93.53%**	**81.27%**
ResNet-18 (L1)	86.74%	61.09%	44.65%	77.66%

Table 5: Ablation study: Regression R^2 for predicting chemical concentration and physical characteristics in tomatoes, bananas, and avocados

Reducing the network depth to 2 layers lowered test accuracy to 94.44% for tomatoes, 82.17% for bananas, and 88.98% for avocados, while increasing it to 4 layers achieved 96.89%, 82.80%, and 88.46%, respectively. Neither model matched the baseline accuracy. Narrowing the filters to 16-32-64 decreased accuracy to 90% for tomatoes, 81.85% for bananas, and 89.32% for avocados. Widening the network improved accuracy for tomatoes (97.03%) and bananas (87.58%) but not avocados (89.32%), suggesting overfitting. Replacing ReLU with LeakyReLU caused only a slight accuracy dip (96.22% for tomatoes, 86.31% for bananas, and 90.17% for avocados), indicating ReLU suffices. Removing dropout reduced training accuracy to 94.44% for tomatoes, 83.76% for bananas, and 88.46% for avocados. Overall, MobiChem delivers optimal results without excessive complexity.

Chemical Concentration and Physical Property Prediction Model. For the chemical concentration and physical property prediction task, we assess the impact of RNC loss on regression performance. Our complete pipeline integrates an encoder with RNC loss followed by a linear regression layer with L1 loss using a shared ResNet-18 backbone. We compare this to a baseline model with a ResNet-18 encoder trained with L1 loss. The results in Table 5 show the advantage of the MobiChem model, with its R^2 values significantly higher than the ResNet-18 model: 97.82% (-0.94%) for lycopene, 61.09% (-34.58%) for chlorophyll, 44.65% (-48.88%) for sugar content in bananas, and 75.23% (-6.04%) for avocado firmness.

Location and Time. We evaluated our system's robustness across different locations and seasons by collecting data from multiple sites over three batches within one year. To assess the impact of ambient light and seasonal changes, we partitioned the data by location and collection time. Locations tested the hardware's ability to block external light, while seasonal variation ensured the system could handle the same fruit species in different conditions. We sampled 10% from each location or batch as a test set. The results, shown in Figure 15, reveal no significant accuracy differences across fruits or conditions, demonstrating that the system is robust to ambient light changes and generalizable across seasons.

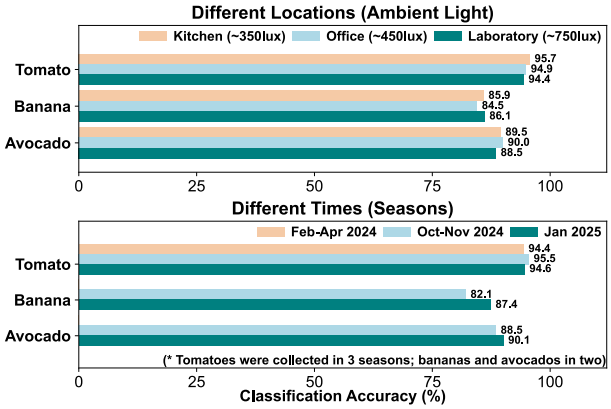

Figure 15: System Evaluation under Varied Conditions

7 RELATED WORKS

Mobile Application in Food Quality Sensing. For food/chemical sensing tasks to mobile devices, there are mainly two directions of implementation: standalone prototypes [20, 24, 25, 27], or incorporation with existing COTS mobile devices [13, 35, 78]. For example, BabyNutri [27] uses a customized printed spectrometer with selected wavelengths, so as to analyze the purity and concentration of liquid food products. CapCam [78] makes use of the vibration-induced ripple of the speaker of the smartphone captured by the camera to measure the alcohol concentration. Although the standalone prototype have more sensor choices, incorporation with smartphone achieves wider ubiquity deployments and better sensing potentials. MobiChem stands out from previous work as it is ubiquitously compatible with most smartphones. Among all smartphone-based implementations for food quality control, to the best of our knowledge, MobiChem is the first work to use an optical filter array, phone screen, and front camera to achieve on-device hyperspectral image captures.

Hyperspectral Imaging System for Food Quality Sensing. Hyperspectral imaging (HSI) has broad sensing capability for food products. Many prior works have been successful in assessing tenderness, water concentration, and possible contamination of meat[17], poultry carcass [11], and fish [38]. Due to the spatial nature of hyperspectral imaging output, Hyperspectral Imaging system assist visualization for the sugar distribution, ripening area, and einsect infecting location of citrus [40], melons[60], and tomatoes [47], etc. However, many of those HSI system empathize more with accuracy over cost and portability. All traditional configurations of a hyperspectral imaging system require expensive optical components and bulky mechanical structures. These gaps limit the costs and mobility of hyperspectral imaging systems, and motivate MobiChem as a low-cost mobile HSI sensing system.

Low-Cost Implementation of Hyperspectral Imaging System. To make hyperspectral imaging system suitable for diverse mobile applications, [32, 45, 51, 61] works focus on optimizing hardware configurations through low-cost and compact components. For example, [61] miniaturizes the 100-spectral band system to the size of a normal image sensor by electronic fabrication of microscopic wedge filter arrays on top of every sensor unit. HyperCam [21] as one of the early low-cost HSI works, provides a low-cost hardware implementation using LEDs to allow faster switching between wavelength channels. Recently, researchers also considered spectral reconstruction from RGB images to hyperspectral images as a computer vision task [4, 36, 69]. Among all models, MST++ [9] by Cai et al. is the latest state-of-the-art model. MST++ pioneers using the vision transformer model (ViT) for spectral reconstruction. MobiSpectral [54] incorporated MST++ as a mobile software on the stand-alone phone-based hyperspectral imaging system. However, MobiSpectral requires IR camera of Pixel 4a and is not practical.

8 DISCUSSION

Generalization Across Different Fruit Types In this paper, we focus on three climacteric fruits: tomatoes, bananas, and avocados. Our approach can naturally extend to other climacteric produce, assuming linear or near-linear correlations between measurable attributes and maturity progression. Such relationships are well-documented in fruits like mangoes and papayas [55]. However, species-specific factors must be considered for robust generalization, as some fruits may have subtler visual or chemical changes requiring more calibration. Despite this, the core MobiChem pipeline—spectral filtering, data processing, and ranking-based regression—is transferrable to other fruits.

Hardware Generalization As shown in Figure 6, MobiChem is easily adaptable to different phone brands. After collecting a small set of phone-specific measurements, replicating the workflow requires minimal effort. With different models, we can create a similar 3D-printed shell and select filters based on the phone's backlight. While demonstrated with one smartphone, our modular, parameter-driven pipeline is universal, making hyperspectral imaging applicable to all COTS smartphones.

9 CONCLUSION

In this paper, we presented MobiChem, a smartphone-based toolkit for practical fruit monitoring. MobiChem utilizes the smartphone's front camera and display, enhanced with a zero-powered screen cover. Combined with deep learning models, it delivers hyperspectral imaging capabilities traditionally limited to costly, bulky equipment. Our experiments on tomatoes, avocados, and bananas demonstrated MobiChem's high performance in fruit monitoring, achieving 95.67% accuracy in chlorophyll measurement, 98.76% in lycopene detection, 93.53% in sugar concentration analysis, and 91.34% average in classifying maturity (96.64% for tomato, 86.37% for banana, and 91.03% for avocado). MobiChem offers an accessible solution for non-destructive fruit monitoring for mobile devices. We believe such an application has the potential to transform daily consumer grocery habits and traditional agricultural practices, as well as enhance food assessment.

ACKNOWLEDGMENT

This research is partially supported by the National Science Foundation (NSF) via Award No. 2403528. Additionally, we appreciate the generous resources and advice on the infographic designs provided by Yimeng Liu, Juexing Wang, and Huaili Zeng. Lastly, we thank all anonymous reviewers and shepherd for their valuable feedback.

REFERENCES

[1] Mahmoud A Abdelhamid, Yuri Sudnik, Haider J Alshinayyin, and Fatma Shaaban. 2021. Non-destructive method for monitoring tomato ripening based on chlorophyll fluorescence induction. *Journal of Agricultural Engineering* 52, 1 (2021).

[2] Sayed Saad Afzal, Atsutse Kludze, Subhajit Karmakar, Ranveer Chandra, and Yasaman Ghasempour. 2023. AgriTera: Accurate Non-Invasive Fruit Ripeness Sensing via Sub-Terahertz Wireless Signals. In *Proceedings of the 29th Annual International Conference on Mobile Computing and Networking*. 1–15.

[3] Lucille Alexander and Don Grierson. 2002. Ethylene biosynthesis and action in tomato: a model for climacteric fruit ripening. *Journal of experimental botany* 53, 377 (2002), 2039–2055.

[4] Boaz Arad, Radu Timofte, Ohad Ben-Shahar, Yi-Tun Lin, and Graham D Finlayson. 2020. Ntire 2020 challenge on spectral reconstruction from an rgb image. In *Proceedings of the IEEE/CVF Conference on Computer Vision and Pattern Recognition Workshops*. 446–447.

[5] Rosa Arias, Tung-Ching Lee, Logan Logendra, and Harry Janes. 2000. Correlation of lycopene measured by HPLC with the L*, a*, b* color readings of a hydroponic tomato and the relationship of maturity with color and lycopene content. *Journal of Agricultural and Food Chemistry* 48, 5 (2000), 1697–1702.

[6] John P. Bower and Jonathan G. Cutting. 1988. Avocado Fruit Development and Ripening Physiology. In *Horticultural Reviews* (1 ed.), Jules Janick (Ed.). Wiley, 229–271. https://doi.org/10.1002/9781118060834.ch7

[7] IR Bunghez, M Raduly, S Doncea, I Aksahin, and RM Ion. 2011. LYCOPENE DETERMINATION IN TOMATOES BY DIFFERENT SPECTRAL TECHNIQUES (UV-VIS, FTIR AND HPLC). *Digest Journal of Nanomaterials & Biostructures (DJNB)* 6, 3 (2011).

[8] Britt M Burton-Freeman and Howard D Sesso. 2014. Whole food versus supplement: comparing the clinical evidence of tomato intake and lycopene supplementation on cardiovascular risk factors. *Advances in Nutrition* 5, 5 (2014), 457–485.

[9] Yuanhao Cai, Jing Lin, Zudi Lin, Haoqian Wang, Yulun Zhang, Hanspeter Pfister, Radu Timofte, and Luc Van Gool. 2022. Mst++: Multi-stage spectral-wise transformer for efficient spectral reconstruction. In *Proceedings of the IEEE/CVF Conference on Computer Vision and Pattern Recognition*. 745–755.

[10] A Carrillo-López and EM Yahia. 2014. Changes in color-related compounds in tomato fruit exocarp and mesocarp during ripening using HPLC-APcI+-mass Spectrometry. *Journal of food science and technology* 51 (2014), 2720–2726.

[11] Kuanglin Chao. 2010. Automated poultry carcass inspection by a hyperspectral–multispectral line-scan imaging system. In *Hyperspectral imaging for food quality analysis and control*. Elsevier, 241–272.

[12] YuTsung Cheng, PingHsiu Huang, YungJia Chan, PoYuan Chiang, WenChien Lu, ChangWei Hsieh, ZengChin Liang, BoWen Yan, ChiunChuang R Wang, and PoHsien Li. 2024. Investigate the composition and physicochemical properties attributes of banana starch and flour during ripening. *Carbohydrate Polymer Technologies and Applications* 7 (2024), 100446.

[13] Anshuman J Das, Akshat Wahi, Ishan Kothari, and Ramesh Raskar. 2016. Ultra-portable, wireless smartphone spectrometer for rapid, non-destructive testing of fruit ripeness. *Scientific reports* 6, 1 (2016), 32504.

[14] Helmut Dislich. 1979. Plastics as optical materials. *Angewandte Chemie International Edition in English* 18, 1 (1979), 49–59.

[15] Mervyn C D'Souza, Suman Singha, and Morris Ingle. 1992. Lycopene Concentration of Tomato Fruit can be Estimated from Chromaticity Values. *HortScience* 27, 5 (1992), 465–466.

[16] Edmund. 2024. 3" x 5" 200 filters, Rosco Color Filter Swatchbook. https://www.edmundoptics.com/p/3quot-x-5quot-200-filters-color-filter-booklet/4470

[17] Gamal ElMasry and Da-Wen Sun. 2010. Meat quality assessment using a hyperspectral imaging system. In *Hyperspectral imaging for food quality analysis and control*. Elsevier, 175–240.

[18] Salaheddin M Elyatem and Adel A Kader. 1984. Post-harvest physiology and storage behaviour of pomegranate fruits. *Scientia Horticulturae* 24, 3-4 (1984), 287–298.

[19] L Ivan Epstein. 1952. The design of optical filters. *JOSA* 42, 11 (1952), 806–810.

[20] Mayank Goel, Eric Whitmire, Alex Mariakakis, T Scott Saponas, Neel Joshi, Dan Morris, Brian Guenter, Marcel Gavriliu, Gaetano Borriello, and Shwetak N Patel. 2015. HyperCam: hyperspectral imaging for ubiquitous computing applications. In *Proceedings of the 2015 ACM International Joint Conference on Pervasive and Ubiquitous Computing*. 145–156.

[21] Mayank Goel, Eric Whitmire, Alex Mariakakis, T. Scott Saponas, Neel Joshi, Dan Morris, Brian Guenter, Marcel Gavriliu, Gaetano Borriello, and Shwetak N. Patel. 2015. HyperCam: Hyperspectral Imaging for Ubiquitous Computing Applications. In *Proceedings of the 2015 ACM International Joint Conference on Pervasive and Ubiquitous Computing* (Osaka, Japan) *(UbiComp '15)*. Association for Computing Machinery, New York, NY, USA, 145–156. https://doi.org/10.1145/2750858.2804282

[22] Juliana Freitas Santos Gomes, Rafaela Rezende Vieira, and Fabiana Rodrigues Leta. 2013. Colorimetric indicator for classification of bananas during ripening. *Scientia Horticulturae* 150 (2013), 201–205.

[23] Antihus Hernández Gómez, Jun Wang, Guixian Hu, and Annia García Pereira. 2008. Monitoring storage shelf life of tomato using electronic nose technique. *Journal of Food Engineering* 85, 4 (2008), 625–631.

[24] Unsoo Ha, Junshan Leng, Alaa Khaddaj, and Fadel Adib. 2020. Food and liquid sensing in practical environments using {RFIDs}. In *17th USENIX Symposium on Networked Systems Design and Implementation (NSDI 20)*. 1083–1100.

[25] Unsoo Ha, Yunfei Ma, Zexuan Zhong, Tzu-Ming Hsu, and Fadel Adib. 2018. Learning food quality and safety from wireless stickers. In *Proceedings of the 17th ACM workshop on hot topics in networks*. 106–112.

[26] Kaiming He, Xiangyu Zhang, Shaoqing Ren, and Jian Sun. 2016. Deep Residual Learning for Image Recognition. In *2016 IEEE Conference on Computer Vision and Pattern Recognition (CVPR)*. 770–778. https://doi.org/10.1109/CVPR.2016.90

[27] Haiyan Hu, Qianyi Huang, and Qian Zhang. 2023. Babynutri: a cost-effective baby food macronutrients analyzer based on spectral reconstruction. *Proceedings of the ACM on Interactive, Mobile, Wearable and Ubiquitous Technologies* 7, 1 (2023), 1–30.

[28] Xiaogang Jiang, Mingwang Zhu, Jinliang Yao, Yuxiang Zhang, and Yande Liu. 2022. Calibration of near infrared spectroscopy of apples with different fruit sizes to improve soluble solids content model performance. *Foods* 11, 13 (2022), 1923.

[29] Tariq Kamal, Shasha Cheng, Imtiaz Ali Khan, Khalid Nawab, Tan Zhang, Yukun Song, Siqi Wang, Muhammad Nadeem, Muhammad Riaz, Malak Atiq Ullah Khan, et al. 2019. Potential uses of LF-NMR and MRI in the study of water dynamics and quality measurement of fruits and vegetables. *Journal of Food Processing and Preservation* 43, 11 (2019), e14202.

[30] Zoi Katsirma, Eirini Dimidi, Ana Rodriguez-Mateos, and Kevin Whelan. 2021. Fruits and their impact on the gut microbiota, gut motility and constipation. *Food & function* 12, 19 (2021), 8850–8866.

[31] Devinder Kaur, Rekhika Sharma, Ali Abas Wani, Balmeet Singh Gill, and D.S. Sogi. 2006. Physicochemical Changes in Seven Tomato (Lycopersicon esculentum) Cultivars During Ripening. *International Journal of Food Properties* 9, 4 (Dec. 2006), 747–757. https://doi.org/10.1080/10942910600575716 Publisher: Taylor & Francis _eprint: https://doi.org/10.1080/10942910600575716.

[32] Alexander Kokka, Hans Toivanen, Rami Mannila, and Antti Näsilä. 2022. High-resolution hyperspectral imager based on tunable fabry-pérot interferometer filter technology. In *Photonic Instrumentation Engineering IX*, Vol. 12008. SPIE, 39–46.

[33] Nobuyuki Kozukue and Mendel Friedman. 2003. Tomatine, chlorophyll, β-carotene and lycopene content in tomatoes during growth and maturation. *Journal of the Science of Food and Agriculture* 83, 3 (2003), 195–200.

[34] Yutong Liu, Landu Jiang, Linghe Kong, Qiao Xiang, Xue Liu, and Guihai Chen. 2021. Wi-Fruit: See through fruits with smart devices. *Proceedings of the ACM on Interactive, Mobile, Wearable and Ubiquitous Technologies* 5, 4 (2021), 1–29.

[35] Yutong Liu, Landu Jiang, Linghe Kong, Qiao Xiang, Xue Liu, and Guihai Chen. 2022. Wi-Fruit: See Through Fruits with Smart Devices. *Proc. ACM Interact. Mob. Wearable Ubiquitous Technol.* 5, 4, Article 169 (dec 2022), 29 pages. https://doi.org/10.1145/3494971

[36] Andreas Lugmayr, Martin Danelljan, Radu Timofte, Kang-wook Kim, Younggeun Kim, Jae-young Lee, Zechao Li, Jinshan Pan, Dongseok Shim, Ki-Ung Song, et al. 2022. NTIRE 2022 challenge on learning the super-resolution space. In *Proceedings of the IEEE/CVF Conference on Computer Vision and Pattern Recognition*. 786–797.

[37] Tharaka Maduwanthi and R. Marapana. 2017. Biochemical changes during ripening of banana: A review. (Sept. 2017).

[38] Paolo Menesatti, Corrado Costa, and Jacopo Aguzzi. 2010. Quality evaluation of fish by hyperspectral imaging. In *Hyperspectral imaging for food quality analysis and control*. Elsevier, 273–294.

[39] Konica Minolta. 2024. CR-300 Chroma Meter. https://sensing.konicaminolta.us/us/products/cr-300-chroma-meter/

[40] Enrique Moltó, José Blasco, and Juan Gómez-Sanchís. 2010. Analysis of hyperspectral images of citrus fruits. In *Hyperspectral imaging for food quality analysis and control*. Elsevier, 321–348.

[41] Loc T Nguyen, Abdullatif Tay, VM Balasubramaniam, JD Legan, Evan J Turek, and Rockendra Gupta. 2010. Evaluating the impact of thermal and pressure treatment in preserving textural quality of selected foods. *LWT-Food Science and Technology* 43, 3 (2010), 525–534.

[42] Jorge A Osuna-García, Gilles Doyon, Samuel Salazar-García, Ricardo Goenaga, and Isidro JL González-Durán. 2011. Relationship between skin color and some fruit quality characteristics of 'Hass' avocado. *Journal of Agriculture of the University of Puerto Rico* 95, 1-2 (2011), 15–23.

[43] Godliver Owomugisha, Pius KB Mugagga, Friedrich Melchert, Ernest Mwebaze, John A Quinn, and Michael Biehl. 2020. A low-cost 3-D printed smartphone add-on spectrometer for diagnosis of crop diseases in field. In *Proceedings of the 3rd ACM SIGCAS Conference on Computing and Sustainable Societies*. 331–332.

[44] Guilhem Pagés, Catherine Deborde, Martine Lemaire-Chamley, Annick Moing, and Jean-Marie Bonny. 2021. MRSI vs CEST MRI to understand tomato metabolism in ripening fruit: is there a better contrast? *Analytical and Bioanalytical Chemistry* 413 (2021), 1251–1257.

[45] Eleftheria Maria Pechlivani, Athanasios Papadimitriou, Sotirios Pemas, Nikolaos Giakoumoglou, and Dimitrios Tzovaras. 2023. Low-Cost Hyperspectral Imaging Device for Portable Remote Sensing. *Instruments* 7, 4 (2023), 32.

[46] B&H photo. 2024. Sekonic C-7000 Spectrometer Color Meter. https://www.bhphotovideo.com/c/product/1199079-REG/sekonic_401_7000_c_7000_spectromaster_color_meter.html/

[47] Gerrit Polder and Gerie van der Heijden. 2010. Measuring ripening of tomatoes using imaging spectrometry. In *Hyperspectral imaging for food quality analysis and control*. Elsevier, 369–402.

[48] Jianwei Qin. 2010. CHAPTER 5 - Hyperspectral Imaging Instruments. In *Hyperspectral Imaging for Food Quality Analysis and Control*, Da-Wen Sun (Ed.). Academic Press, San Diego, 129–172. https://doi.org/10.1016/B978-0-12-374753-2.10005-X

[49] Jose L Ramirez-GarciaLuna, Mario A Martinez-Jimenez, Robert DJ Fraser, Robert Bartlett, Amy Lorincz, Zheng Liu, Gennadi Saiko, and Gregory K Berry. 2023. Is my wound infected? A study on the use of hyperspectral imaging to assess wound infection. *Frontiers in Medicine* 10 (2023), 1165281.

[50] A Venket Rao and Sanjiv Agarwal. 2000. Role of antioxidant lycopene in cancer and heart disease. *Journal of the American College of Nutrition* 19, 5 (2000), 563–569.

[51] Jairo Salazar-Vazquez and Andres Mendez-Vazquez. 2020. A plug-and-play Hyperspectral Imaging Sensor using low-cost equipment. *HardwareX* 7 (2020), e00087.

[52] Rob E Schouten, Brian Farneti, LMM Tijskens, A Algarra Alarcón, and Ernst J Woltering. 2014. Quantifying lycopene synthesis and chlorophyll breakdown in tomato fruit using remittance VIS spectroscopy. *Postharvest biology and technology* 96 (2014), 53–63.

[53] Dasom Seo, Byeong-Hyo Cho, and Kyoung-Chul Kim. 2021. Development of monitoring robot system for tomato fruits in hydroponic greenhouses. *Agronomy* 11, 11 (2021), 2211.

[54] Neha Sharma, Muhammad Shahzaib Waseem, Shahrzad Mirzaei, and Mohamed Hefeeda. 2023. MobiSpectral: Hyperspectral Imaging on Mobile Devices. In *Proceedings of the 29th Annual International Conference on Mobile Computing and Networking*. 1–15.

[55] Sirithon Siriamornpun and Niwat Kaewseejan. 2017. Quality, bioactive compounds and antioxidant capacity of selected climacteric fruits with relation to their maturity. *Scientia Horticulturae* 221 (2017), 33–42.

[56] Panmanas Sirisomboon, Munehiro Tanaka, and Takayuki Kojima. 2012. Evaluation of tomato textural mechanical properties. *Journal of Food Engineering* 111, 4 (2012), 618–624.

[57] Mahmoud Soltani, Reza Alimardani, Mahmoud Omid, and Iran Karaj. 2011. Changes in physico-mechanical properties of banana fruit during ripening treatment. *Journal of american Science* 7, 5 (2011), 14–19.

[58] MB Stuart, M Davies, C Fisk, E Allen, AJ Sole, R Ing, MJ Hobbs, and JR Willmott. 2024. Smartphone-based hyperspectral imaging for ice sheet and proglacial applications in South-West Greenland. *Science of The Total Environment* 951 (2024), 175516.

[59] Mary B Stuart, Andrew JS McGonigle, Matthew Davies, Matthew J Hobbs, Nicholas A Boone, Leigh R Stanger, Chengxi Zhu, Tom D Pering, and Jon R Willmott. 2021. Low-cost hyperspectral imaging with a smartphone. *Journal of Imaging* 7, 8 (2021), 136.

[60] Junichi Sugiyama and Mizuki Tsuta. 2010. Visualization of sugar distribution of melons by hyperspectral technique. In *Hyperspectral imaging for food quality analysis and control*. Elsevier, 349–368.

[61] Nicolaas Tack, Andy Lambrechts, Philippe Soussan, and Luc Haspeslagh. 2012. A compact, high-speed, and low-cost hyperspectral imager. In *Silicon Photonics VII*, Vol. 8266. SPIE, 126–138.

[62] Taobao. 2024. 490 nm filter (Chinese). https://item.taobao.com/item.htm?_u=120d953uvo9d76&id=617534673475&spm=a1z09.2.0.0.2e402e8dLEZkOt

[63] Taobao. 2024. 510 nm filter (Chinese). https://item.taobao.com/item.htm?_u=120d953uvo8ae1&id=43183165428&spm=a1z09.2.0.0.2e402e8dLEZkOt

[64] Taobao. 2024. 550 nm filter (Chinese). https://item.taobao.com/item.htm?_u=120d953uvo9193&id=673568887529&spm=a1z09.2.0.0.2e402e8dLEZkOt

[65] Taobao. 2024. 570 nm filter (Chinese). https://item.taobao.com/item.htm?_u=120d953uvo31ac&id=39587209721&spm=a1z09.2.0.0.2e402e8dLEZkOt

[66] Taobao. 2024. 590 nm filter (Chinese). https://item.taobao.com/item.htm?_u=120d953uvo5e1f&id=520424386814&spm=a1z09.2.0.0.2e402e8dLEZkOt

[67] Taobao. 2024. Optical Filter Vender (Chinese). https://shop61874463.taobao.com/

[68] Shimeles Tilahun, Mu Hong Seo, In Geun Hwang, Seok Hyeon Kim, Han Ryul Choi, Cheon Soon Jeong, et al. 2018. Prediction of lycopene and β-carotene in tomatoes by portable chroma-meter and VIS/NIR spectra. *Postharvest biology and technology* 136 (2018), 50–56.

[69] Radu Timofte, Shuhang Gu, Jiqing Wu, and Luc Van Gool. 2018. Ntire 2018 challenge on single image super-resolution: Methods and results. In *Proceedings of the IEEE conference on computer vision and pattern recognition workshops*. 852–863.

[70] Leon Amadeus Varga, Jan Makowski, and Andreas Zell. 2021. Measuring the ripeness of fruit with hyperspectral imaging and deep learning. In *2021 International Joint Conference on Neural Networks (IJCNN)*. IEEE, 1–8.

[71] Dhruv Verma, Ian Ruffolo, David B Lindell, Kiriakos N Kutulakos, and Alex Mariakakis. 2024. ChromaFlash: Snapshot Hyperspectral Imaging Using Rolling Shutter Cameras. *Proceedings of the ACM on Interactive, Mobile, Wearable and Ubiquitous Technologies* 8, 3 (2024), 1–31.

[72] PK Verma, P Pathak, B Kumar, H Himani, and P Preety. 2023. Automatic Optical Imaging System for Mango Fruit Using Hyperspectral Camera and Deep Learning Algorithm. *IJRITCC* 11 (2023), 112–117.

[73] Jose A Villa-Rodríguez, F Javier Molina-Corral, J Fernando Ayala-Zavala, Guadalupe I Olivas, and Gustavo A González-Aguilar. 2011. Effect of maturity stage on the content of fatty acids and antioxidant activity of 'Hass' avocado. *Food Research International* 44, 5 (2011), 1231–1237.

[74] Alley E Watada, Karl H Norris, JOHN T WORTHINGTON, and DAVIS R MASSIE. 1976. Estimation of chlorophyll and carotenoid contents of whole tomato by light absorbance technique. *Journal of Food Science* 41, 2 (1976), 329–332.

[75] Brett B Wedding, Carole Wright, Steve Grauf, Paul Gadek, and Ronald D White. 2019. The application of FT-NIRS for the detection of bruises and the prediction of rot susceptibility of 'Hass' avocado fruit. *Journal of the Science of Food and Agriculture* 99, 4 (2019), 1880–1887.

[76] Denise Wilson. 2019. *Sensing the Perfect Tomato: An Internet of Sensing Approach*. CRC Press.

[77] Xujun Ye, Tomoki Izawa, and Shuhuai Zhang. 2018. Rapid determination of lycopene content and fruit grading in tomatoes using a smart device camera. *Cogent Engineering* 5, 1 (2018), 1504499.

[78] Shichao Yue and Dina Katabi. 2019. Liquid testing with your smartphone. In *Proceedings of the 17th Annual International Conference on Mobile Systems, Applications, and Services*. 275–286.

[79] Huaili Zeng, Gen Li, and Tianxing Li. 2024. PyroSense: 3D Posture Reconstruction Using Pyroelectric Infrared Sensing. *Proc. ACM Interact. Mob. Wearable Ubiquitous Technol.* 7, 4, Article 197 (Jan. 2024), 32 pages. https://doi.org/10.1145/3631435

[80] Kaiwen Zha, Peng Cao, Jeany Son, Yuzhe Yang, and Dina Katabi. 2023. Rank-N-Contrast: Learning Continuous Representations for Regression. In *Advances in Neural Information Processing Systems*, A. Oh, T. Naumann, A. Globerson, K. Saenko, M. Hardt, and S. Levine (Eds.), Vol. 36. Curran Associates, Inc., 17882–17903. https://proceedings.neurips.cc/paper_files/paper/2023/file/39e9c5913c970e3e49c2df629daff636-Paper-Conference.pdf

[81] Hongyan Zhu, Bingquan Chu, Yangyang Fan, Xiaoya Tao, Wenxin Yin, and Yong He. 2017. Hyperspectral Imaging for Predicting the Internal Quality of Kiwifruits Based on Variable Selection Algorithms and Chemometric Models. *Scientific Reports* 7, 1 (Aug. 2017), 7845. https://doi.org/10.1038/s41598-017-08509-6